From deuterons to neutron stars: variations in nuclear many-body theory

R. B. Wiringa

Physics Division, Argonne National Laboratory, Argonne, Illinois 60439

A major goal in nuclear physics is to understand the stability, structure, and reactions of nuclei as a consequence of the interactions between individual nucleons. This colloquium describes one attempt to build a consistent picture of nuclear systems ranging in size from deuterons to neutron stars. The main ingredients are a nonrelativistic Hamiltonian containing two- and three-nucleon interactions, and correlated variational wave functions as approximate solutions of the many-body Schrödinger equation. A model that fits both two-body scattering data and nuclear masses will provide the best theoretical input for neutron star properties.

CONTENTS

I. INTRODUCTION

The systematics of nuclear binding energies is among the most important pieces of empirical knowledge in nuclear physics. It summarizes an important aspect of nuclear physics for the rest of science: that significant energy will be released if two small nuclei are joined together (fusion) or if one large nucleus is split into two smaller fragments (fission). This is the basis for energy production in stars, the chemical evolution of the universe, and for nuclear reactors and weapons on earth.

The binding energy $B(Z,N)$ of a nucleus with Z protons and N neutrons is the mass difference between free nucleons and the bound nucleus:

$$B(Z,N)=[Zm_p+Nm_n-m_{\rm nuc}(Z,N)]c^2 . \quad (1)$$

A plot of the maximum binding energy per nucleon of stable nuclei, $B_{\rm max}(Z,N)/A$, versus the number of nucleons, $A=Z+N$, is shown in Fig. 1. There is a rapid rise from low A to a maximum of 8.8 MeV in the region $A=56-62$ and, finally, a gradual decline to 7.9 MeV by $A=208$. This function, commonly called the curve of binding energy, is generally smooth, but there are local spikes or peaks at certain values of Z or N: the magic numbers 2, 8, 20, 28, 50, 82, and 126. Historically, the relatively constant value of $B_{\rm max}/A$ was the first evidence for the short range of nuclear forces (Bethe and Bacher, 1936), and the magic numbers inspired the development of the nuclear shell model (Mayer and Jensen, 1955).

The general characteristics of the curve of binding energy have been known for over 50 years. Over the same period of time our knowledge of the interactions between individual nucleons has grown and is now quite extensive. Considerable theoretical efforts have been made on a continuing basis to understand nuclear masses in terms of the forces between individual nucleons, but a detailed quantitative explanation is still lacking. In this colloquium we describe one attempt to build a consistent picture of nuclear systems in the context of a nonrelativistic Hamiltonian containing realistic two- and three-body potentials, using correlated variational wave functions as approximate solutions to the many-body Schrödinger equation.

We aim at understanding both the absolute energies and the relative stability of nuclei and the origin of features such as spin-orbit splitting in the nuclear shell model. What we learn is applicable to areas not directly accessible to experiment, such as the study of neutron stars. The surface of neutron stars consists of neutron-rich nuclei, which we cannot create in the laboratory, while the neutron star core is a nucleon fluid 5 times denser than that in the interior of stable nuclei. Nevertheless, our ability to model neutron stars is directly related to our ability to account for known nuclear masses from nuclear interactions.

A key feature of nuclear physics is that a realistic nucleon-nucleon (NN) potential, i.e., a potential that gives a good fit to data from experiments involving only two nucleons, must have a complicated operator structure. Beyond the NN potential good evidence exists for significant many-body forces which require us to introduce three-nucleon (NNN) potentials to obtain quantitatively correct nuclear masses and spin-orbit splittings. Nuclear many-body calculations have thus proved quite formidable, but substantial progress has been made in recent years.

Sections II and III describe the Hamiltonian and outline the variational method for solving the many-body Schrödinger equation. Sections IV–VI discuss details of our calculations for few-body nuclei, closed-shell nuclei, and the nuclear matter expected to be found in the interior of the heaviest nuclei and neutron stars. Section VII shows how this information is used to construct neutron star models.

II. HAMILTONIAN

The first step in developing a useful microscopic picture of nuclear structure is obtaining a practical model

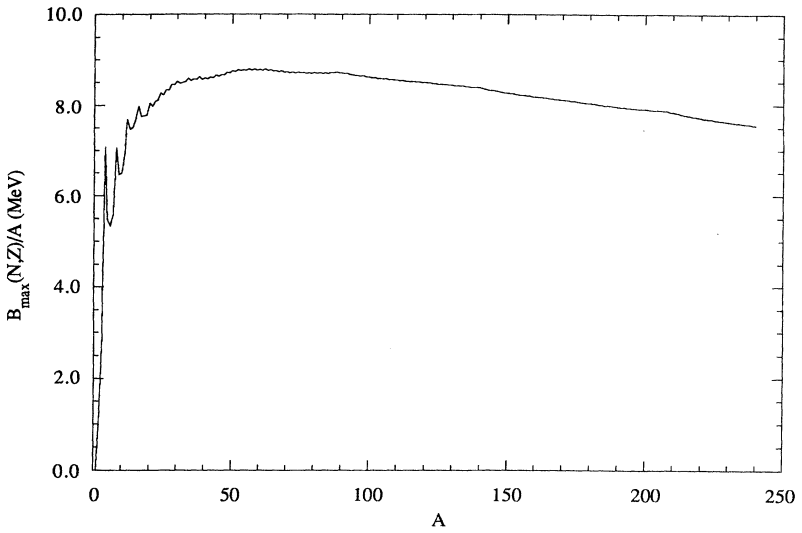

FIG. 1. Binding-energy curve.

for the forces between nucleons. Quantum chromodynamics (QCD) is the currently accepted theory of the strong force; however, it is extremely difficult to use in the nonperturbative regime appropriate for nuclear structure, and most work with QCD has been limited to characterizing the structure of individual baryons. Calculations for nucleon-nucleon interactions using a quark model description give some of the known qualitative features, such as the strong repulsive core, but the quantitative fits to data are poor (see, for example, Myhrer and Wroldsen, 1988). The meson-exchange theory of nuclear forces has been more successful—not directly as a strongly coupled quantum field theory, which cannot be applied rigorously, but more as a guide to developing the form of potential models. In this approach, nucleons, nucleon resonances such as the $\Delta(1232)$, and mesons, such as the π, ρ, and ω, are incorporated in a potential representation, and various parameters in the potential are adjusted to fit *NN* elastic-scattering and bound-state data (Lacombe *et al.*, 1980; Machleidt *et al.*, 1987).

One might question both the validity and the utility of a potential representation for composite objects whose individual structure is ultimately described by a quantum field theory. One justification for this approach can be made by analogy; a similar approach has been very successful in studies of atomic ^{4}He and ^{3}He quantum liquids and solids. Helium atoms themselves are composite objects whose electronic structure is determined by quantum electrodynamics (QED). However, describing the interaction of two or more helium atoms directly by QED is impractical. Instead, electronic structure calculations can be used to guide the development of atom-atom potentials, which are then fit to two-body (virial and transport coefficient) data (Aziz *et al.*, 1979). Accurate solutions of the many-body Schrödinger equation for such potentials have been obtained; they reproduce many experimental properties, including the binding energy as a function of density for liquid and solid ^{4}He (Kalos *et al.*, 1981), the binding energy of liquid ^{3}He (Lee *et al.*, 1981), the low-lying excitation spectrum of ^{4}He (Manousakis and Pandharipande, 1984), and even the superfluid λ transition (Ceperley and Pollock, 1986).

Meson-exchange theory predicts a complicated operator structure for the *NN* potential, which is confirmed in practice when fitting *NN* data. It also predicts complicated interactions among three or more nucleons which cannot be represented by iterated *NN* potentials, implying a need for *NNN* (and possibly higher-order) potentials in many-nucleon systems. With this as a guide, we take for the nuclear Hamiltonian

$$H=\frac{-\hbar^2}{2m}\sum_i \nabla_i^2+\sum_{i<j} v_{ij}+\sum_{i<j<k} V_{ijk}\ . \tag{2}$$

The *NN* potential v_{ij} is constrained to fit *NN* elastic-scattering data and deuteron properties, while the *NNN* potential V_{ijk} is constrained by fitting properties of heavier nuclear systems.

The meson-theoretic basis for v_{ij} is illustrated in Fig. 2. The dominant long-range interaction is due to one-pion exchange, with the nonrelativistic potential reduction

$$v_{ij}^{\pi}=\frac{f_{\pi NN}^2}{4\pi}\frac{m_\pi}{3}X_{ij}^{\pi}\tau_i\cdot\tau\ , \tag{3}$$

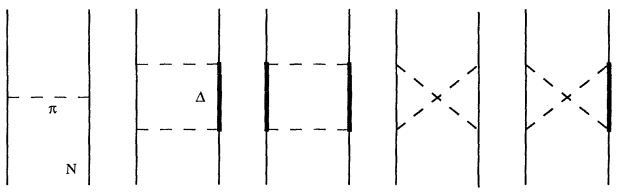

FIG. 2. Processes contributing to the *NN* potential. Solid lines represent nucleons, dashed lines represent pion exchange, and heavy solid lines denote the nucleon resonance $\Delta(1232)$.

$$X_{ij}^{\pi} = Y_{\pi}(r_{ij})\sigma_i\cdot\sigma_j + T_{\pi}(r_{ij})S_{ij} \ , \tag{4}$$

where $f_{\pi NN}^2$ is the πNN coupling constant, σ and τ are the usual Pauli spin and isospin operators, and $S_{ij}=[3(\sigma_i\cdot\hat{\mathbf{r}}_{ij})(\sigma_j\cdot\hat{\mathbf{r}}_{ij})-\sigma_i\sigma_j]$ is the tensor operator. The Yukawa and tensor functions have the asymptotic behavior $Y(r\to\infty)=\exp(-\mu r)/\mu r$, $T(r\to\infty)=[1+3/\mu r+3/(\mu r)^2]Y(r)$, with $\mu=m_{\pi}/\hbar c$. At intermediate distances two-pion exchange is the dominant process, with the possible excitation of intermediate nucleon resonances. Analysis with interaction models that include the strong $\Delta(1232)$ resonance as an additional degree of freedom shows that these processes provide significant attraction, which can be characterized by a predominantly central force with some weaker spin-, isospin-, and tensor-dependent terms. At shorter distances, the interaction, which becomes strongly repulsive, may be attributed to the exchange of heavier mesons, such as the ρ and ω, and/or to the quark substructure of nucleons. In addition, momentum-dependent terms appear due to nonlocalities and relativistic terms in the meson exchange.

In practice, when NN elastic-scattering data are analyzed, the interaction is found to depend strongly on the total spin S (=0,1) and isospin T (=0,1) of the pair of nucleons. The fact that only the $S,T=(1,0)$ np system has a bound state (the deuteron or ^{2}H) also confirms the spin and isospin dependence. Further, the deuteron has a finite electric quadrupole moment, implying a nonspherical ground state and a tensor force. The dependence of the $S,T=(1,1)$ P-wave phase shifts on the total angular momentum implies both tensor and short-range spin-orbit ($\mathbf{L}\cdot\mathbf{S}$) forces.

One useful representation for a realistic v_{ij} is a sum of operators:

$$v_{ij} = \sum_{p=1,n} v_p(r_{ij})O_{ij}^p \ , \tag{5}$$

where the $v_p(r_{ij})$ are radial functions of the pair separation $|\mathbf{r}_i-\mathbf{r}_j|$, and the number n of the operators O_{ij}^p is as large as necessary to fit the data. A minimum of eight operators is required to fit the deuteron and S- and P-wave elastic-scattering data; they are commonly chosen as

$$O_{ij}^{p=1,8} = 1,\ \tau_i\cdot\tau_j,\ \sigma_i\cdot\sigma_j,\ (\sigma_i\cdot\sigma_j)(\tau_i\cdot\tau_j),\ S_{ij},\ S_{ij}(\tau_i\cdot\tau_j),\ \mathbf{L}\cdot\mathbf{S},\ \mathbf{L}\cdot\mathbf{S}(\tau_i\cdot\tau_j) \ . \tag{6}$$

(We shall sometimes use the more descriptive labels c, τ, σ, $\sigma\tau$, t, $t\tau$, ls, and $ls\tau$ for these operators.) The numerical results described in this paper were computed with the Argonne v_{14} potential (Wiringa *et al.*, 1984), which has six operators quadratic in $\mathbf{L}$ in addition to the eight operators of Eq. (6). Other well-known potentials, such as the Nijmegen (Nagels *et al.*, 1978), Paris (Lacombe *et al.*, 1980), and Bonn (Machleidt *et al.*, 1987) models, include the same basic eight operators and four to ten additional terms (quadratic in $\mathbf{p}$ and/or $\mathbf{L}$) that are needed to get quantitatively accurate fits to high partial-wave NN scattering data. The degree of dependence on S and T is illustrated in Fig. 3, which shows the four possible S,T combinations (linear combinations of the c, τ, σ, and $\sigma\tau$ operators) of the Argonne model.

Realistic models for the NNN potential also have a complicated operator structure. Some meson-exchange diagrams that contribute to V_{ijk} are shown in Fig. 4. The

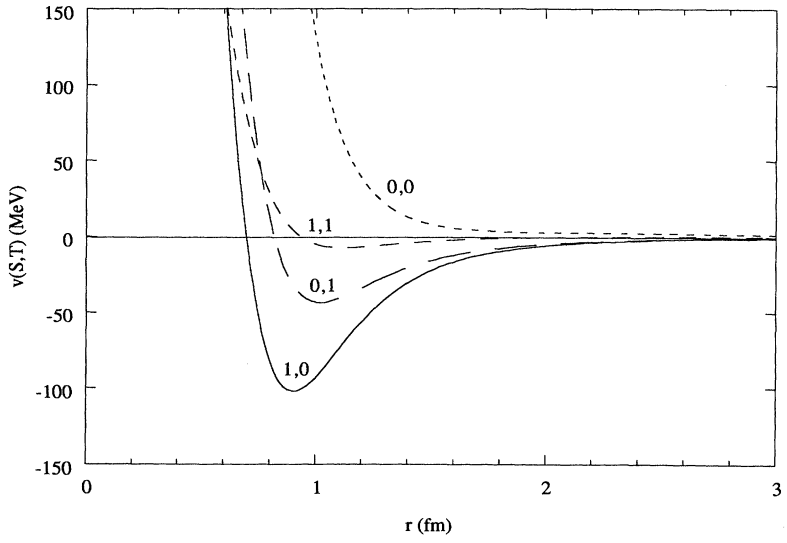

FIG. 3. Dependence of the Argonne v_{14} NN potential on total spin S and isospin T.

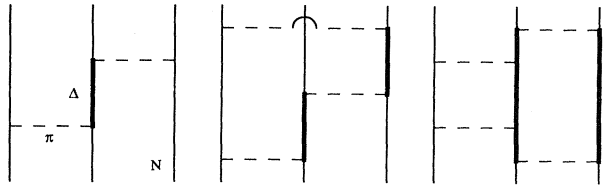

FIG. 4. Processes contributing to the *NNN* potential. Solid lines represent nucleons, dashed lines represent pion exchange, and heavy solid lines denote the nucleon resonance Δ(1232).

longest-ranged part stems from two-pion exchange between three nucleons, with an intermediate nonnucleonic state. The most important intermediate state is the Δ(1232), which leads to an *NNN* potential with the operator structure (Fujita and Miyazawa, 1957)

$$V_{ijk}^{2\pi}=A\sum_{\text{cyc}}\left(\{X_{ij}^{\pi},X_{jk}^{\pi}\}\{\tau_i\cdot\tau_j,\tau_j\cdot\tau_k\}+\tfrac{1}{4}[X_{ij}^{\pi},X_{jk}^{\pi}][\tau_i\cdot\tau_j\cdot\tau_k]\right). \quad (7)$$

Here A is a factor involving πNN and $\pi N\Delta$ coupling constants; X_{ij}^{π} is the one-pion exchange operator of Eq. (4); and a cyclic sum is made over the indices i, j, and k. Theoretical analysis of πN scattering data has led to more complete two-pion-exchange potentials, such as the Tucson-Melbourne model (Coon *et al.*, 1979). In practice, it is useful to add a shorter-range repulsive term V_{ijk}^{R}, which is expected both from studies of models with explicit Δ(1232) resonances (Hadjuk *et al.*, 1983) and from relativistic corrections (Carlson *et al.*, 1992). Numerical results presented here have been obtained for two versions of the Urbana V_{ijk}, in which a phenomenological V_{ijk}^{R} without spin or isospin dependence is used (Carlson *et al.*, 1983). Adding V_{ijk} to H yields additional binding in light nuclei, where the attractive two-pion exchange dominates, and more rapid saturation in nuclear matter from the shorter-range repulsion.

III. MANY-BODY THEORY

The complicated operator structure of realistic v_{ij} and V_{ijk} models makes solution of the many-nucleon problem difficult. A great deal of effort has gone into the development of methods for solving the many-body Schrödinger equation with such potentials. These include Faddeev techniques for few-body systems (Chen *et al.*, 1986; Ishikawa and Sasakawa, 1986; Stadler *et al.*, 1991), coupled-cluster calculations for closed-shell nuclei (Kümmel *et al.*, 1978), and Brueckner-Bethe-Goldstone methods for nuclear matter (Day, 1981). A general approach used to study all these systems, from few-body nuclei to dense nucleon matter, is the variational theory with correlation operators (Pandharipande and Wiringa, 1979; Lomnitz-Adler *et al.*, 1981; Wiringa *et al.*, 1988; Pieper *et al.*, 1990). A single basic ansatz with correlations generated by the interactions serves to construct the trial wave function Ψ_v for all systems. This method gives an approximate solution to the many-body Schrödinger equation adequate for many purposes and provides the best solution currently available in cases such as dense matter. It can also serve as a starting point for more exact methods, such as the Green's-function Monte Carlo (GFMC) procedure (Carlson, 1988), which projects out the exact ground state by stochastically evaluating the limit $|\Psi_0\rangle=\lim_{\tau\to\infty}\exp(-H\tau)|\Psi_v\rangle$.

The variational method involves the construction of Ψ_v and the evaluation of the energy expectation value,

$$E_v=\frac{\langle\Psi_v|H|\Psi_v\rangle}{\langle\Psi_v|\Psi_v\rangle}\geq E_0\ . \quad (8)$$

Parameters in Ψ_v are varied to obtain the lowest possible upper bound E_v to the ground-state energy E_0. This optimal Ψ_v is then an approximate solution of the many-body Schrödinger equation and can be used to evaluate other expectation values of interest. Excited or scattering-state solutions are also obtained for the lowest-lying states of a given set of quantum numbers. The keys to successful application of the variational method are a realistic and flexible ansatz for the trial function and accurate methods for evaluating expectation values.

A realistic trial function must reflect the complicated operator structure of the nuclear Hamiltonian. A good ansatz for the trial function consists of a correlated operator product acting on a Jastrow wave function:

$$|\Psi_v\rangle=\left[\mathcal{S}\prod_{i<j<k}(1+U_{ijk})\right]\left[\mathcal{S}\prod_{i<j}(1+u_{ij})\right]|\Psi_J\rangle\ , \quad (9)$$

$$|\Psi_J\rangle=\prod_{i<j}f_c(r_{ij})\mathcal{A}|\Phi\rangle\ . \quad (10)$$

Here Φ indicates a single-particle state with appropriate properties for the system of interest, such as the quantum numbers $JMTT_3$ for a particular nucleus. The $f_c(r)$ is a radial pair-correlation function, while the u_{ij} are pair-correlation operators with the same structure as v_{ij}:

$$u_{ij}=\sum_{p=2,8}u_p(r_{ij})O_{ij}^{p}\ . \quad (11)$$

The operators O_{ij}^{p} are the same as in Eq. (6). The U_{ijk} are triplet correlations induced by V_{ijk}, and $\mathcal{A}$ and $\mathcal{S}$ represent antisymmetrization and symmetrization operators.

For few-body nuclei, we use a single-particle Φ with spin-isospin variables and no spatial dependence; for example, for ^{4}He,

$$|\Phi_\alpha\rangle=|\uparrow p\ \downarrow p\ \uparrow n\ \downarrow n\rangle\ , \quad (12)$$

where the first particle is a spin-up proton, etc. For closed-shell nuclei such as ^{16}O and ^{40}Ca, Φ is conveniently expressed as a product of four determinants:

$$|\Phi_{\rm O}\rangle=D_{\uparrow p}D_{\downarrow p}D_{\uparrow n}D_{\downarrow n}\ . \quad (13)$$

For ^{16}O, each determinant is constructed from one 1s and three 1p single-particle wave functions, $\phi_{lm}(r_i)$, for a par-

ticle bound in a well. For infinite matter, we use a product of plane-wave states with spin-isospin quantum numbers, i.e., the Fermi-gas wave function

$$\Phi=\prod_i \phi_i=\prod_i \exp(i\mathbf{k}_i\cdot\mathbf{r}_i)\chi_i\nu_i \ , \tag{14}$$

where χ_i and ν_i represent spin and isospin states.

The central $f_c(r)$ and noncentral $u_p(r)$ pair correlations reflect the influence of v_{ij} at short distances while satisfying certain asymptotic boundary conditions. They are generated from a set of eight coupled differential equations (Lagaris and Pandharipande, 1981a). For example, the linear combination $f_c(r)[1+u_\tau(r)-3u_\sigma(r)-3u_{\sigma\tau}(r)]\equiv f_{ST=01}(r)$ is obtained by solving the Euler-Lagrange equation:

$$\frac{-\hbar^2}{m}\nabla^2 f_{01}(r)+[\bar{v}_{01}(r)-\lambda_{01}(r)]f_{01}(r)=0 \ . \tag{15}$$

Here $\bar{v}_{01}$ is a quenched version of the bare NN potential, obtained by multiplying the noncentral components v_p by a parameter $\alpha<1$, and λ_{01} is a parametrized Lagrange multiplier adjusted to fit boundary conditions. The short-range boundary condition is $f_{ST}(r\to 0)=$constant, while the long-range boundary condition depends on the system. For few-body nuclei all the spatial confinement is provided by the radial dependence of the pair-correlation functions, with $[f_{ST}(r\to\infty)]^{A-1}\propto\exp(-\kappa_{ST}r)/r$, where $\hbar^2\kappa_{ST}^2/m=e_{ST}$ is a separation energy parameter. No spatial confinement is required for infinite nuclear or neutron matter. Nucleons separated by large distances are uncorrelated; so $f_{ST}(r\to\infty)=1$. For closed-shell nuclei, nuclear matter boundary conditions are used for $f_{ST}(r)$, and the confined structure of Ψ_v is built into the single-particle wave functions $\phi_{lm}(r_i)$.

Representative correlation functions for ^{2}H, ^{4}He, ^{16}O, and nuclear matter are shown in Fig. 5. The $f_c(r)$ is small at short distances and peaks at an intermediate distance, which reduces (maximizes) contributions from the repulsive core (intermediate-range attraction) of v_{ij}. The $u_p(r)$ are all relatively small, and only the most important of these, $u_{t\tau}$, is shown. The exact deuteron wave function can be written in terms of a wave function containing only $f_c(r)$ and $u_{t\tau}(r)$. The $f_c(r)$ are very similar at short distances, while their long-range behavior varies according to the boundary conditions discussed above. The $u_{t\tau}(r)$, and other $u_p(r)$ not shown, are also remarkably similar for all systems.

The method used to evaluate the energy expectation value varies with the size of the system under consideration. For finite nuclei, Monte Carlo (MC) techniques are used for spatial integrations. For few-body nuclei, $A\le 8$, a complete sum over spin-isospin states is possible, but for larger nuclei the number of spin-isospin degrees of freedom becomes too large and a cluster expansion is required. For nuclear and neutron star matter a cluster expansion is also used, but with integral equations to sum terms.

IV. FEW-BODY NUCLEI

The Metropolis Monte Carlo algorithm (Metropolis *et al.*, 1953) is a standard method for evaluating multidimensional integrals efficiently by spending more computational effort where the integrand is largest, as determined by an appropriate probability density, or weight

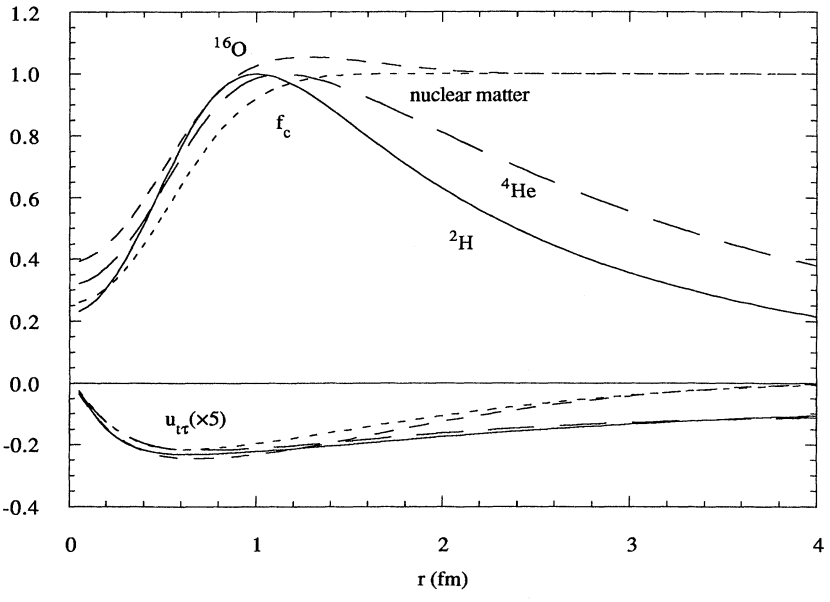

FIG. 5. Correlation functions f_c and $u_{t\tau}$ for ^{2}H, ^{4}He, ^{16}O, and nuclear matter.

function, such as $|\Psi|^2$. Nuclear problems meet a unique difficulty caused by the complicated operator dependence of both the interactions and the wave function, which requires summing over the spin and isospin degrees of freedom.

The Monte Carlo energy expectation value involves a sum over configurations $\{\mathbf{R},p,q\}$:

$$\langle H\rangle=\frac{\sum[\langle\Psi_p^\dagger(\mathbf{R})H\Psi_q(\mathbf{R})\rangle/W_{pq}(\mathbf{R})]}{\sum[\langle\Psi_p^\dagger(\mathbf{R})\Psi_q(\mathbf{R})\rangle/W_{pq}(\mathbf{R})]}\ . \tag{16}$$

A complete sum over all spin-isospin states is made at each configuration specified by the coordinates $\mathbf{R}=(\mathbf{r}_1,\mathbf{r}_2,\ldots,\mathbf{r}_A)$ and by the orders p and q of pair operators in the symmetrized product of Eq. (9). The weight function $W_{pq}(\mathbf{R})=|\langle\tilde{\Psi}_p^\dagger(\mathbf{R})\tilde{\Psi}_q(\mathbf{R})\rangle|$, where $\tilde{\Psi}$ is the trial function Ψ without u_{ls} or U_{ijk} correlations which are expensive to compute. The Metropolis algorithm produces a set of configurations $\{\mathbf{R},p,q\}$ whose density is proportional to this probability distribution. The expectation value can be made arbitrarily exact within a statistical error estimated by the standard deviation, which decreases as the reciprocal square root of the number of statistically independent samples.

The wave function $\Psi(\mathbf{R})$ can be represented by an array of $N_S\times N_T$ complex numbers, where N_S and N_T are the number of spin and isospin basis states: $N_S=2^A$ in the basis of definite S_z, while N_T is smaller because both T and T_3 are conserved. The operators $O_{ij}^{p=1,6}$ contained in u_{ij} and H are represented by sparse matrices in this basis. Kinetic energy and gradient terms in the L-dependent parts of v_{ij} are calculated by numerical differences using slightly shifted positions. The main computational task lies in constructing Ψ and $H\Psi$ for many different configurations $\{\mathbf{R},p,q\}$ (Carlson and Wiringa, 1991). The overall effort required is proportional to the product of the array size for Ψ, the number of pairs and triples in the system, and the number of positions required for evaluating gradients, all of which grow rapidly with A. To calculate the binding energy with a reasonable statistical error for one trial function requires only two minutes for ^{3}H, but nearly two hours for ^{6}Li on one processor of a Cray-YMP.

Experimental values and variational results for the energies of ^{3}H and ^{4}He for the Argonne v_{14}+Urbana VIII Hamiltonian are shown in Table I (Wiringa, 1991). Shown also are the results of essentially exact three-body Faddeev (Chen *et al.*, 1990) and four-body GFMC calculations (Carlson, 1990), which are 3–4 % below the variational bounds. A realistic v_{ij} alone underbinds ^{3}H by $\approx$1 MeV and ^{4}He by $\approx$5 MeV. A plausible V_{ijk} can be added to get the correct binding; the Urbana VIII potential was adjusted to fit the experimental ^{3}H energy in the exact Faddeev calculation, when used in conjunction with the Argonne v_{14} model. The ^{4}He energy then comes out correctly in its exact GFMC calculation.

Results for ^{5}He and ^{6}Li are shown in Table II. There is no stable five-body nucleus; ^{5}He is a neutron-^{4}He P-wave scattering state with possible total angular momenta of $J=\frac{3}{2}$ or $\frac{1}{2}$. The phase shift as a function of energy can be calculated variationally by placing the particles in a box with appropriate asymptotic boundary conditions and varying the interior wave function to minimize the energy (Carlson *et al.*, 1987). The boundary condition used here corresponds to an experimental scattering energy in the $J=\frac{3}{2}$ ($\frac{1}{2}$) state of 1.1 (2.5) MeV. The energy difference of 1.4 MeV between these two scattering states is the spin-orbit splitting. The variational calculation for Argonne v_{14}+Urbana VIII is 2.1 (3.1) MeV above the variational energy for ^{4}He, while a recent GFMC calculation gives 1.5 (2.7) MeV more than its ^{4}He energy (Carlson and Wiringa, 1992). Thus the variational calculation gets 70% of the spin-orbit splitting, while the GFMC calculation gets 85%, for this Hamiltonian. Approximately half of the splitting comes from the V_{ijk}.

Experimentally, six-body nuclei such as ^{6}He and ^{6}Li are very weakly bound systems. At present the best variational trial functions do not give stability against breakup into smaller pieces for this Hamiltonian. The ^{6}Li result shown here is for a trial function in which the variational parameters have been constrained to give the empirical charge radius. It is more bound than ^{4}He, but

TABLE I. Binding energy (in MeV) for three- and four-body nuclei. Numbers in parentheses are one-standard-deviation Monte Carlo error estimates in the last significant figure.

Nucleus	Hamiltonian	Method	Binding energy
^{3}H	nature	experiment	8.48
	Argonne v_{14}	variational MC	7.45(1)
		34-ch. Faddeev	7.67
	Argonne v_{14}	variational MC	8.21(2)
	plus Urbana VIII	34-ch. Faddeev	8.49
^{4}He	nature	experiment	28.3
	Argonne v_{14}	variational MC	23.5(1)
	Argonne v_{14}	variational MC	27.2(1)
	plus Urbana VIII	GFMC	28.3(2)

TABLE II. Binding and separation energies (in MeV) for five- and six-body nuclei. Numbers in parentheses are one-standard-deviation Monte Carlo error estimates in the last significant figure.

Nucleus	Hamiltonian	Method	Binding energy	Separation energy
^{5}He ($j=\frac{3}{2}$)	nature	experiment	27.2	-1.1 ($\alpha+n$)
	Argonne v_{14}	variational MC	25.1(1)	-2.1
	plus Urbana VIII	GFMC	26.8(2)	-1.5
^{5}He ($j=\frac{1}{2}$)	nature	experiment	25.8	-2.5 ($\alpha+n$)
	Argonne v_{14}	variational MC	24.1(2)	-3.1
	plus Urbana VIII	GFMC	25.6(2)	-2.7
^{6}Li	nature	experiment	32.0	1.5 ($\alpha+d$)
	Argonne v_{14}	variational MC	27.8(3)	-1.9
	plus Urbana VIII			

not more bound than separated ^{4}He and ^{2}H nuclei. No GFMC results are available at present for six-body or larger nuclei with realistic interactions.

V. CLOSED-SHELL NUCLEI

Because of the rapid growth with A in computational expense of the direct MC integration, an alternative method for evaluating expectation values is needed in larger systems. To reduce the amount of spin-isospin computation, we use a cluster expansion for the noncentral correlation operators u_{ij} and U_{ijk} to evaluate expectation values. For example,

$$\left\langle \sum_{i<j} v_{ij} \right\rangle = \frac{\sum_{i<j} n_{ij} + \sum_{i<j<k} n_{ijk} + \cdots + n_{12\cdots A}}{1+\sum_{i<j} d_{ij} + \sum_{i<j<k} d_{ijk} + \cdots + d_{12\cdots A}} \equiv \sum_{i<j} c_{ij} + \sum_{i<j<k} c_{ijk} + \cdots + c_{12\cdots A} \ . \quad (17)$$

Each numerator term $n_{ij}\ldots$ or denominator term $d_{ij}\ldots$ represents an A-body integral in which only nucleons $ij\cdots$ are connected by interactions or correlation operators u_{ij} and U_{ijk}:

$$n_{ij} = \langle \Psi_J | (1+u_{ij}^\dagger) v_{ij} (1+u_{ij}) | \Psi_J \rangle \ , \quad (18)$$

$$d_{ij} = \langle \Psi_J | (1+u_{ij}^\dagger)(1+u_{ij}) | \Psi_J \rangle - 1 \ . \quad (19)$$

The brackets denote here a full $3A$-dimensional integration that treats the central correlations and antisymmetry of the Jastrow wave function completely. However, the computational effort is much reduced because the spin-isospin algebra is needed only for the particles in the cluster that have correlation operators. The terms are grouped in a convergent linked-cluster expansion, e.g., $c_{ij} = n_{ij}/(1+d_{ij})$. The expectation values of the individual cluster terms, $n_{ij}\ldots$, $d_{ij}\ldots$, are evaluated using the same MC techniques as for few-body nuclei. The energy evaluation reported below still required some 80 hours of Cray-2 time after the trial function had been optimized.

The cluster expansion would not be useful unless it converged rapidly. The kinetic and two-body potential-energy contributions are, in fact, well converged at the four-body cluster level in ^{16}O, with net contributions of 34.4 and -39.6 MeV/nucleon, respectively. The three-body potential contribution does not converge as rapidly, but alternate groupings of cluster terms lead to the same result, -2.5 MeV/nucleon, which is a third of the net energy of -7.7 MeV/nucleon (Pieper *et al.*, 1992).

Cluster Monte Carlo (CMC) results for the closed-shell nuclei ^{16}O and ^{40}Ca are shown in Table III. The Hamiltonian is Argonne v_{14}+Urbana VII, an earlier member of the series of Urbana models that is somewhat more attractive than the Urbana VIII model used above in few-body nuclei. With this model the binding energy of ^{16}O is close to the experimental value, but is only 0.1 MeV/nucleon more bound than ^{4}He with this interaction. The corresponding experimental difference is 0.9 MeV/nucleon. The CMC result for ^{40}Ca is also very close to experiment, but its trial function has not been

TABLE III. Binding and cluster separation energy (in MeV/A) for closed-shell nuclei. Numbers in parentheses are one-standard-deviation Monte Carlo error estimates in the last significant figure.

Nucleus	Hamiltonian	Method	Binding energy	Separation energy
^{16}O	nature	experiment	8.0	0.9 (4α)
	Argonne v_{14}	cluster MC	7.7(1)	0.1(1)
	plus Urbana VII			
^{40}Ca	nature	experiment	8.5	1.4 (10α)
	Argonne v_{14}	cluster MC	8.6(1.5)	1.0
	plus Urbana VII			

searched thoroughly and the MC statistical error is large.

The spin-orbit splitting can also be examined in the light nuclei. Removal of one proton from the $p_{1/2}$ ($p_{3/2}$) orbital in ^{16}O will give ^{15}N in the $J=\frac{1}{2}$ ($\frac{3}{2}$) ground (excited) state. The energy difference of these two states has been calculated directly, assuming that the remaining correlations in the ^{16}O wave function are unchanged. The calculated difference is 6.1 ± 0.4 MeV, compared to the experimental value of 6.3 MeV. Half of the splitting stems from the two-nucleon spin-orbit and other L-dependent parts of v_{ij}, and half from iterated tensor parts of v_{ij} in three-nucleon clusters and from $V_{ijk}^{2\pi}$ (Pieper and Pandharipande, 1992). This result is in qualitative agreement with earlier Brueckner G-matrix calculations (Ando and Bando, 1981).

VI. NUCLEAR AND NEUTRON MATTER

The general shape of the curve of binding energy is well reproduced by the semiempirical mass formula

$$B(N,Z)=E_0 A-E_s A^{2/3}-E_\beta\frac{(N-Z)^2}{A}-E_C\frac{Z^2}{A^{1/3}}-\frac{\delta}{A^{1/2}}\ , \tag{20}$$

where the terms on the right-hand side are identified as volume (E_0) and surface (E_s) energies, in analogy with a liquid drop, supplemented by symmetry (E_β), Coulomb (E_C), and pairing (δ) terms. Nuclear matter may be viewed as the idealization of an infinite system of equal numbers of neutrons and protons ($N=Z$) at uniform density, without Coulomb interactions. The first goal of nuclear matter calculations is to obtain E_0, whose empirical value is -16 ± 1 MeV/A, and the saturation density ρ_0, which is inferred from nuclear charge-density distributions measured in elastic electron-scattering experiments to be 0.16 ± 0.01 fm^{-3}. Calculations of asymmetric ($N\neq Z$) matter can be used to obtain E_β, and of semi-infinite slabs of nuclear matter to obtain E_s; the empirical values are about 30 MeV/A and 20 MeV/$A^{2/3}$, respectively.

Variational nuclear matter expectation values are evaluated using a diagrammatic cluster expansion and Fermi-hypernetted-chain (FHNC) and single-operator-chain (SOC) integral equations (Pandharipande and Wiringa, 1979). A key aspect of the cluster expansion is the appearance of significant contributions from unlinked diagrams due to the noncommuting correlation operators in Ψ_v. Expectation values are approximated by expanding both the numerator and the denominator of Eq. (8) in powers of the short-range functions

$$F_c(r_{ij})=f_c^2(r_{ij})-1\ ,$$

$$F_p(r_{ij})=2f_c^2(r_{ij})u_p(r_{ij})O_{ij}^p\ ,$$

and

$$F_{pq}(r_{ij})=f_c^2(r_{ij})u_p(r_{ij})u_q(r_{ij})O_{ij}^pO_{ij}^q\ .$$

Three-body correlations have not yet been introduced into variational calculations of nuclear matter. For simplicity the single-particle Φ in Ψ_v is antisymmetrized on only one side of Eq. (8), and the contribution of exchanges is reduced to powers of the Slater function $l(k_Fr_{ij})=3j_1(k_Fr_{ij})/k_Fr_{ij}$ with a sum over $O_{ij}^{p=1-4}$. The expansion is conveniently described in terms of generalized Mayer diagrams with dynamic (F_c,F_p,F_{pq}) and exchange (l and l^2) correlation links.

The FHNC/SOC integral equations sum certain classes of diagrams in the cluster expansion to infinite order in the number of particles. These equations are an extension of the hypernetted-chain (HNC) integral equation developed for Bose systems, such as liquid atomic ^{4}He (van Leeuwen *et al.*, 1959). The nature of these equations can be illustrated by considering the pair distribution function $g(r)$, which is the probability of finding a particle at a distance r from a given particle. It can be expressed exactly as

$$g(r)\equiv\frac{1}{A\rho}\langle\delta(r-r_{ij})\rangle=f_c^2(r)\exp[G(r)+E(r)]\ , \tag{21}$$

where $G(r)$ and $E(r)$ are sums of composite and elementary diagram classes. $G(r)$, whose leading contribution is a three-body diagram, results from the two-dimensional integral equation

$$G(r_{ij})=\rho\int[g(r_{ik})-1-G(r_{ik})][g(r_{jk})-1]d^3r_k\ . \tag{22}$$

The leading contribution to $E(r)$, stemming from a four-body diagram, will be small if the F_c are short-ranged. The HNC approximation is to neglect $E(r)$, and Eq. (22) is referred to as the HNC equation when the substitution $g(r)=f_c^2(r)\exp[G(r)]$ is made. In Fermi systems such as liquid atomic ^{3}He, keeping track of different exchange terms requires the specification of four subclasses of composite diagrams, $G_{xy}(r_{ij})$, where the labels x and y specify whether particles i and j have been exchanged or not. There are also various subclasses of elementary diagrams, which the FHNC approximation neglects, leaving a set of four coupled integral equations to be solved for the $G_{xy}(r_{ij})$ (Fantoni and Rosati, 1975).

The pair distribution function of Eq. (21) generalizes to an operator g_{ij} in nuclear matter:

$$g_{ij}=\sum_{p=1,6}g_p(r_{ij})O_{ij}^p\ . \tag{23}$$

The SOC approximation for $g_p(r)$ involves diagrams with a single chain of operator correlations, F_p and/or F_{pq}, with additional hypernetted F_c and exchange links. Each noncentral term requires an additional five coupled integral equations, giving a total of 29 coupled integral equations similar to Eq. (22) in the FHNC/SOC approximation. These are solved iteratively in parallel (Pandharipande and Wiringa, 1979).

The g_{ij} serves to evaluate expectation values of operators; e.g.,

$$\left\langle\sum_{p=1,6}v_p(r_{ij})O_{ij}^p\right\rangle=\rho\sum_{p=1,6}\int v_p(r_{ij})g_p(r_{ij})C([O_{ij}^p]^2)d^3r_{ij}\ . \tag{24}$$

Only the constant or C part of the product of operators $[O_{ij}^p]^2$ contributes after summation over spins and isospins. L-dependent terms in the potential are somewhat more complicated and are calculated only through the three-body cluster level. Some terms in the kinetic energy, as well as V_{ijk}, require a three-body distribution function $g_3(r_{ij},r_{ik},r_{jk})$; a good approximation to this is built from products of the $g_p(r)$.

Variational results for the binding energy of nuclear matter as a function of density for the Argonne v_{14} potential, alone and with the Urbana VII potential are shown in Fig. 6 (Wiringa *et al.*, 1988). The empirical curve represents $E(\rho)=E_0+\frac{1}{18}[(\rho-\rho_0)/\rho_0]^2K$, with the incompressibility K estimated to be 210 MeV/nucleon from an analysis of breathing mode oscillations in finite nuclei induced by inelastic α scattering. Shown also are the best available Brueckner-Bethe-Goldstone (BBG) calculations for v_{ij}, which lie 1–2 MeV below the variational bounds (Day and Wiringa, 1985). No BBG calculations have been made with realistic V_{ijk}.

The Argonne v_{14} potential alone saturates matter at about the correct energy, but at almost twice the empirical density. Variational and BBG calculations with other v_{ij} give very similar results. Thus nuclear matter is overbound in contrast to light nuclei, which are underbound. The addition of V_{ijk} radically alters the saturation properties of nuclear matter; the repulsive short-range part of the Urbana VII model used here moves the saturation density close to its empirical value, although with insufficient binding. The variational expectation value of the energy is probably accurate within 1 MeV at ρ_0, but the lack of three-body correlations implies a trial function inferior to that used in few-body and light nuclei. We estimate the exact saturation point for Argonne v_{14} plus Urbana VII at $E_0\approx -15$ MeV/nucleon for $\rho_0\approx 0.19$ fm^{-3} and $K\approx 240$ MeV/nucleon.

A pure neutron matter calculation is a simple variant of the nuclear matter calculation described above. In this case, the operator $\tau_i\cdot\tau_j$ equals unity, requiring only half as many v_p, u_p, and g_p terms, obtained as sums of the isospin-dependent and isospin-independent terms, e.g., $\bar{v}_c=v_c+v_\tau$. Calculations of asymmetric matter with a fixed proton fraction $x=\rho_p/\rho$ are more difficult, but detailed studies have shown this energy to be well approximated by

$$E(\rho,x)=T_F(\rho,x)+V_0(\rho)+(1-2x)^2V_2(\rho)\ , \tag{25}$$

$$T_F(\rho,x)=\frac{3\hbar^2}{10m}(3\pi^2\rho)^{2/3}[x^{5/3}+(1-x)^{5/3}]\ . \tag{26}$$

$T_F(\rho,x)$ is the Fermi-gas kinetic energy, while the functions $V_0(\rho)$ and $V_2(\rho)$ are obtained from the results of symmetric nuclear matter ($x=\frac{1}{2}$) and pure neutron matter ($x=0$) calculations (Lagaris and Pandharipande, 1981b). The symmetry energy is then

$$E_\beta(\rho)=\tfrac{5}{9}T_F(\rho,\tfrac{1}{2})+V_2(\rho)\ . \tag{27}$$

The Argonne v_{14} plus Urbana VII Hamiltonian yields $E_\beta=29$ MeV/A at ρ_0, in good agreement with the empirical value.

The approximation of Eq. (25) facilitates estimating the energy and proton fraction for β-stable matter in the interior of neutron stars, where neutrons and protons are in equilibrium with electrons and muons through the reactions $n\Longleftrightarrow p+e^-\Longleftrightarrow p+\mu^-$. One simply requires balancing the chemical potentials $\mu_x=\partial E/\partial N_x$:

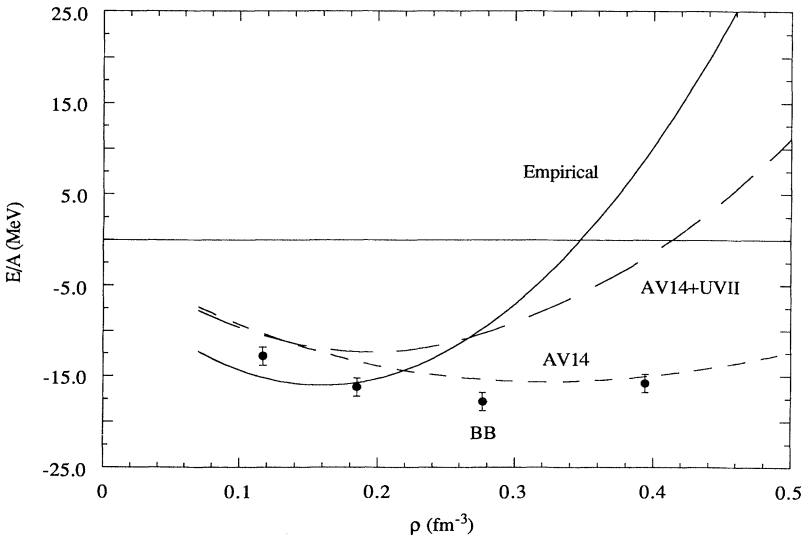

FIG. 6. Nuclear matter energy for Argonne v_{14} (plus Urbana VII) potential in variational (dashed curves) and Brueckner-Bethe (BB, points with error bars) calculations, and the empirical saturation (solid) curve.

$$\mu_n-\mu_p=\tfrac{5}{3}T_F(\rho,\tfrac{1}{2})[(1-x)^{2/3}-x^{2/3}]+4(1-2x)V_2(\rho)$$
$$=\mu_e=[m_e^2+\hbar^2(3\pi^2\rho x_e)^{2/3}]^{1/2}$$
$$=\mu_\mu=[m_\mu^2+\hbar^2(3\pi^2\rho x_\mu)^{2/3}]^{1/2}\ , \qquad (28)$$

with the subsidiary condition $x=x_e+x_\mu$ for charge neutrality. These equations can be solved numerically to obtain x at any density as well as $E(\rho,x)$, once $V_2(\rho)$ is known.

Results for nuclear and neutron matter calculations up to $5\rho_0$ are shown in Fig. 7, along with β-stable matter, the noninteracting neutron Fermi gas $[T_F(\rho,0)]$, and asymmetric matter at $x=\frac{1}{3}$. The latter is appropriate for studies of supernovae, being the approximate proton fraction in the iron core of a massive star just before collapse.

It is important to note that the energy difference between interacting and noninteracting neutron matter is small throughout this density range. This small net interaction energy indicates that nucleons are the relevant degrees of freedom for typical neutron stars where central densities do not exceed $5\rho_0$. The best guide to the physics of high-density matter is thus our knowledge of nuclear interactions through NN scattering data and nuclear masses. A consistent theoretical framework yielding correct values of these quantities will have the best chance of predicting neutron star properties.

VII. NEUTRON STARS

The structure of a neutron star is controlled by the equation of state for β-stable matter, with the bulk of the star being at nuclear matter density or higher. The equation of state $P(\varepsilon)$ gives the pressure P that matter can support for a given mass-energy density ε. This function is obtained from the calculation of β-stable matter via the relations

$$\varepsilon=\rho[E(\rho,x)+mc^2]\ , \qquad (29)$$

$$P=\rho^2\frac{\partial E(\rho,x)}{\partial\rho}\ . \qquad (30)$$

The high-density equation of state (EOS) must be extended down to the density of iron, drawing on nuclear and atomic physics beyond our scope. Stellar structure is determined from the general relativistic equation of hydrostatic balance (Oppenheimer and Volkoff, 1939)

$$\frac{\partial P(r)}{\partial r}=-G\frac{[\varepsilon(r)+P(r)/c^2][m(r)+4\pi r^3P(r)/c^2]}{[1-2Gm(r)/rc^2]r^2}\ , \qquad (31)$$

$$m(r)=\int_0^r 4\pi r'^2\varepsilon(r')dr'\ . \qquad (32)$$

Its solution is obtained by selecting values of the central density $\varepsilon_c\equiv\varepsilon(r=0)$ and its corresponding P_c and integrating outward to a radius R at which $P(r)$ vanishes. This R represents the stellar radius, and $M_G\equiv m(R)$ its gravitational mass. We can also calculate other quantities, such as the binding energy, moment of inertia I, surface redshift z, and amu mass M_A:

$$M_A=m_A\int_0^R\frac{4\pi r^2\rho(r)}{[1-2Gm(r)/rc^2]^{1/2}}dr\ , \qquad (33)$$

where m_A represents one atomic mass unit (1.66×10^{-24} g). The difference M_A-M_G is the stellar binding energy. The properties of a typical neutron star predicted by the

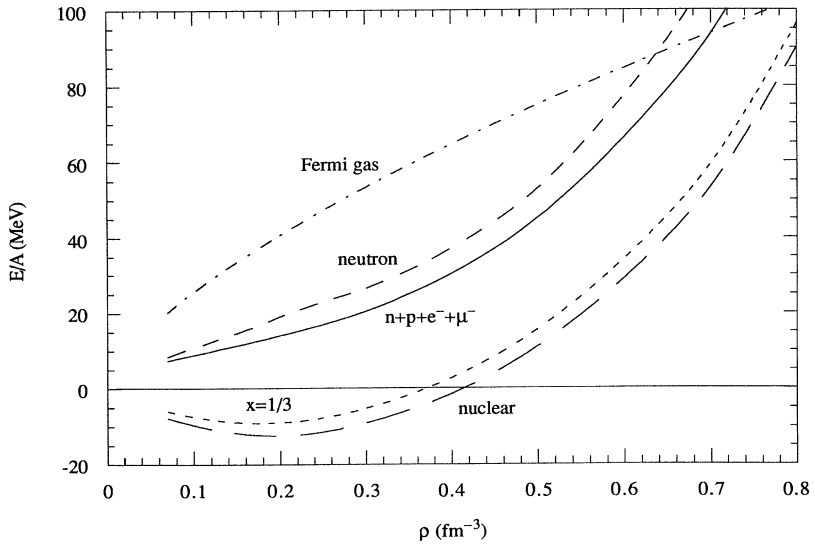

FIG. 7. Energy for dense nucleon matter. The Argonne v_{14} plus Urbana VII interaction is used to calculate nuclear and neutron matter, β-stable matter ($n+p+e^-+\mu^-$), and asymmetric matter at $x=\frac{1}{3}$. Shown also is the energy for a noninteracting Fermi gas of neutrons.

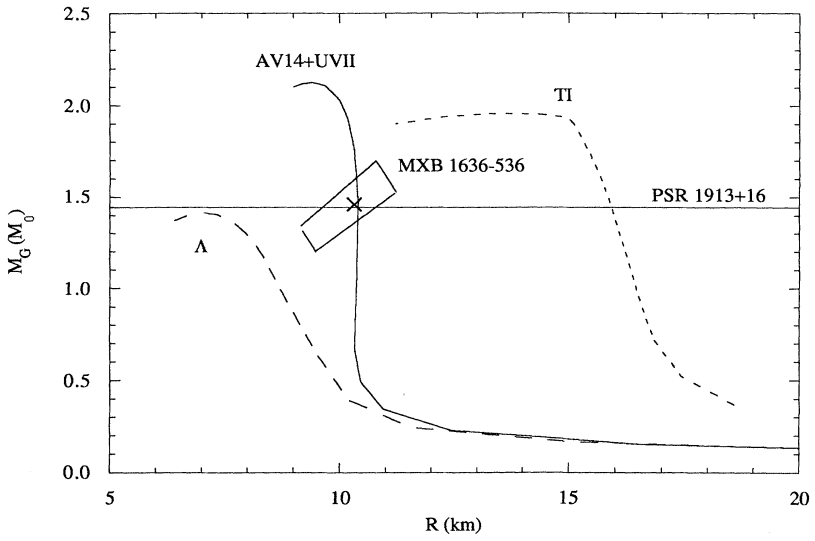

FIG. 8. Gravitational mass $M_G(R)$ calculated for the Argonne v_{14} plus Urbana VII model and the hyperon (Λ) and tensor interaction (TI) models. Shown also (as a straight line) is the mass of radio pulsar PSR 1913+16 and the mass and radius (as a cross with error box) of x-ray burst source MXB 1636-536.

Argonne v_{14} plus Urbana VII model are given in Table IV. The gravitational mass as a function of radius, $M_G(R)$, is shown in Fig. 8 (Wiringa *et al.*, 1988).

Many other theoretical EOS have been developed over the years, two of which are shown in Fig. 8 to indicate the range of predictions (see Arnett and Bowers, 1977, for a larger selection). The hyperon (Λ) model (Pandharipande, 1971) is a "soft" EOS, while the tensor interaction (TI) model (Pandharipande and Smith, 1975) is a "stiff" EOS. As ε_c is increased, R decreases, and M_G rises monotonically to a peak value before turning over. This peak value of M_G is the maximum mass that the given EOS can support; a star with higher central density would be unstable against gravitational collapse to a black hole. Thus a critical test for any theoretical EOS is that its maximum mass be at least as large as that of observed neutron stars. The three models shown here have maximum masses between 1.4 and 2.2 $M_\odot$ (solar masses).

Fairly accurate masses are known for seven radio pulsars, the best measured being PSR 1916+13 at 1.44 $M_\odot$ (Taylor and Weisberg, 1989). This mass is shown in Fig. 8 by a straight line. Another half-dozen x-ray pulsar masses have been estimated, some as high as 1.8 $M_\odot$, but with a large uncertainty (Joss and Rappaport, 1984). The EOS for noninteracting neutrons can support a maximum mass of only 0.7 $M_\odot$, dramatic proof of the importance of nuclear interactions for neutron stars. The large difference in maximum masses between the interacting and noninteracting systems might seem surprising, given the small difference in the energies shown in Fig. 7. However, $P(\varepsilon)$ is the relevant quantity, and it is very different for the interacting and noninteracting curves. Some interacting EOS, such as the hyperon (Λ) model, also fail to support the observed mass of PSR 1913+16 and must be ruled out. Additional EOS models can be discarded if a higher-mass star is confirmed.

Shown also in Fig. 8, as a cross with an error box, is the result of an analysis of data from the x-ray burst source MXB 1636-536, which gives both the mass and the radius of the star (Fujimoto and Taam, 1986). The Argonne v_{14} plus Urbana VII EOS runs right through this point, but the relevant analysis is controversial and additional studies of this kind are needed. New data and a better understanding of radiation emission from neutron stars will, it is hoped, lead to more stringent and reliable constraints.

TABLE IV. Properties of a typical neutron star from the Argonne v_{14} plus Urbana VII model.

ρ_c	0.66 fm^{-3} ($=4.1\rho_0$)
ε_c	1.2×10^{15} g cm^{-3}
P_c	2.1×10^{35} dyn cm^{-2}
M_G	1.4 $M_\odot$
$M_A - M_G$	0.18 $M_\odot$
R	10.4 km
I	1.2×10^{45} g cm^2
z	0.29

VIII. CONCLUSIONS

We have described a series of variational calculations of binding energies of finite and infinite nuclear systems. Many other properties of nuclei, such as density and momentum distributions (Schiavilla *et al.*, 1986), electromagnetic form factors (Schiavilla *et al.*, 1989), and low-energy electroweak reactions (Schiavilla *et al.*, 1992), have been calculated using the same approach. These and other calculations clearly demonstrate that v_{ij} mod-

els constrained by NN data alone are inadequate for yielding quantitative agreement with data in many-nucleon systems. The introduction of a plausible V_{ijk} model leads to a significant improvement in calculated binding energies and spin-orbit splittings of light nuclei, and in the saturation density of nuclear matter. The V_{ijk} also has important consequences for dense matter and neutron stars. An important goal of current research is to further constrain possible models for V_{ijk}, particularly the spin and isospin dependence of its short-range repulsion, by calculating binding energies and spin-orbit splittings of light (and neutron-rich) nuclei between ^{6}Li and ^{16}O. Progress in the study of neutron star structure is closely linked with our understanding of finite nuclei.

ACKNOWLEDGMENTS

The work described here has been carried out in collaboration with many colleagues over a number of years, particularly J. Carlson, A. Fabrocini, I. E. Lagaris, V. R. Pandharipande, S. C. Pieper, R. Schiavilla, and R. A. Smith. Computations have been made at the National Energy Research Supercomputer Center in Livermore, California, and at the National Center for Supercomputing Applications in Champaign, Illinois. This work is supported by the U.S. Department of Energy, Nuclear Physics Division, under Contract No. W-31-109-ENG-38.

REFERENCES

Ando, K., and H. Bando, 1981, Prog. Theor. Phys. **66**, 227.
Arnett, W. D., and R. L. Bowers, 1977, Astrophys. J. Suppl. Ser. **33**, 415.
Aziz, R. A., V. P. S. Nain, J. S. Carley, W. L. Taylor, and G. T. McConville, 1979, J. Chem. Phys. **70**, 4330.
Bethe, H. A., and R. F. Bacher, 1936, Rev. Mod. Phys. **8**, 82.
Carlson, J., 1988, Phys. Rev. C **38**, 1879.
Carlson, J., 1990, Nucl. Phys. A **508**, 141c.
Carlson, J., V. R. Pandharipande, and R. Schiavilla, 1992, "Variational Monte Carlo calculations of ^{3}H and ^{4}He with a relativistic Hamiltonian," University of Illinois Department of Physics Preprint No. ILL-(TH)-92-11.
Carlson, J., V. R. Pandharipande, and R. B. Wiringa, 1983, Nucl. Phys. A **401**, 59.
Carlson, J., K. E. Schmidt, and M. H. Kalos, 1987, Phys. Rev. C **36**, 27.
Carlson, J., and R. B. Wiringa, 1991, in *Computational Nuclear Physics I,* edited by K. Langanke, J. A. Maruhn, and S. E. Koonin (Springer-Verlag, Berlin), p. 171.
Carlson, J., and R. B. Wiringa, 1992, unpublished.
Ceperley, D. M., and E. L. Pollock, 1986, Phys. Rev. Lett. **56**, 351.
Chen, C. R., G. L. Payne, J. L. Friar, and B. F. Gibson, 1986, Phys. Rev. C **33**, 1740.
Chen, C. R., G. L. Payne, J. L. Friar, and B. F. Gibson, 1990, private communication.
Coon, S. A., M. D. Scadron, P. C. McNamee, B. R. Barrett, D. W. E. Blatt, and B. H. J. McKellar, 1979, Nucl. Phys. A **317**, 242.
Day, B. D., 1981, Phys. Rev. C **24**, 1203.
Day, B. D., and R. B. Wiringa, 1985, Phys. Rev. C **32**, 1057.
Fantoni, S., and S. Rosati, 1975, Nuovo Cimento A **25**, 593.
Fujimoto, M. Y., and R. Taam, 1986, Astrophys. J. **305**, 246.
Fujita, J., and H. Miyazawa, 1957, Prog. Theor. Phys. **17**, 360.
Hadjuk, C., P. U. Sauer, and W. Strueve, 1983, Nucl. Phys. A **405**, 581.
Ishikawa, S., and T. Sasakawa, 1986, Few-Body Syst. **1**, 3.
Joss, P. C., and S. A. Rappaport, 1984, Annu. Rev. Astron. Astrophys. **22**, 537.
Kalos, M. H., M. A. Lee, P. A. Whitlock, and G. V. Chester, 1981, Phys. Rev. B **24**, 115.
Kümmel, H., K. H. Lührmann, and J. G. Zabolitzky, 1978, Phys. Rep. C **36**, 1.
Lacombe, M., B. Loiseau, J. M. Richard, R. Vinh Mau, J. Côté, P. Pirès, and R. de Tourreil, 1980, Phys. Rev. C **21**, 861.
Lagaris, I. E., and V. R. Pandharipande, 1981a, Nucl. Phys. A **359**, 349.
Lagaris, I. E., and V. R. Pandharipande, 1981b, Nucl. Phys. A **369**, 470.
Lee, M. A., K. E. Schmidt, M. H. Kalos, and G. V. Chester, 1981, Phys. Rev. Lett. **46**, 728.
Lomnitz-Adler, J., V. R. Pandharipande, and R. A. Smith, 1981, Nucl. Phys. A **361**, 399.
Machleidt, R., K. Holinde, and Ch. Elster, 1987, Phys. Rep. **149**, 1.
Manousakis, E., and V. R. Pandharipande, 1984, Phys. Rev. B **30**, 5062.
Mayer, M. G., and J. H. D. Jensen, 1955, *Elementary Theory of Nuclear Shell Structure* (Wiley, New York).
Metropolis, N., A. W. Rosenbluth, M. N. Rosenbluth, A. H. Teller, and E. Teller, 1953, J. Chem. Phys. **21**, 1087.
Myhrer, F., and J. Wroldsen, Rev. Mod. Phys. **60**, 629.
Nagels, M. M., T. A. Rijken, and J. J. de Swart, 1978, Phys. Rev. D **17**, 768.
Oppenheimer, J. R., and G. M. Volkoff, 1939, Phys. Rev. **55**, 374.
Pandharipande, V. R., 1971, Nucl. Phys. A **178**, 123.
Pandharipande, V. R., and R. A. Smith, 1975, Nucl. Phys. A **237**, 507.
Pandharipande, V. R., and R. B. Wiringa, 1979, Rev. Mod. Phys. **51**, 821.
Pieper, S. C., and V. R. Pandharipande, 1992, "The origins of spin-orbit splitting in ^{15}N," Argonne National Laboratory Physics Division Preprint No. PHY-7106-TH-92.
Pieper, S. C., R. B. Wiringa, and V. R. Pandharipande, 1990, Phys. Rev. Lett. **64**, 364.
Pieper, S. C., R. B. Wiringa, and V. R. Pandharipande, 1992, Phys. Rev. C **46**, 1741.
Schiavilla, R., V. R. Pandharipande, and D. O. Riska, 1989, Phys. Rev. C **40**, 2294.
Schiavilla, R., V. R. Pandharipande, and R. B. Wiringa, 1986, Nucl. Phys. A **449**, 219.
Schiavilla, R., R. B. Wiringa, V. R. Pandharipande, and J. Carlson, 1992, Phys. Rev. C **45**, 2628.
Stadler, A., W. Glöckle, and P. U. Sauer, 1991, Phys. Rev. C **44**, 2319.
Taylor, J. H., and J. M. Weisberg, 1989, Astrophys. J. **345**, 434.
van Leeuwen, J. M. J., J. Groeneveld, and J. de Boer, 1959, Physica (Utrecht) **25**, 792.
Wiringa, R. B., 1991, Phys. Rev. C **43**, 1585.
Wiringa, R. B., V. Fiks, and A. Fabrocini, 1988, Phys. Rev. C **38**, 1010.
Wiringa, R. B., R. A. Smith, and T. L. Ainsworth, 1984, Phys. Rev. C **29**, 1207.